Journal of Engineering and Sustainable Development
Vol. 22, No. 4, July 2018
ISSN 2520-0917
https://doi.org/10.31272/jeasd.2018.4.10

ELECTRICAL AND OPTICAL EFFECTS OF Ag DOPANT ON ZnO THIN FILM BASED MSM UV PHOTODETECTORS

Mohammed Wesam Naji[1] , *Dr. Ghusoon Mohsin Ali[2], Dr. Muneer Aboud Hashem[3]

1) M.Sc, Ministry of Water Resources, Baghdad, Iraq.
2) Asst. Prof., Electrical Engineering Department, Mustansiryah University, Baghdad, Iraq.
3) Asst. Prof., Electrical Engineering Department, Mustansiryah University, Baghdad, Iraq.

Abstract: This paper presents the fabrication, characterization and performance analysis of Zinc Oxide (ZnO) and Sliver doped Zinc Oxide (SZO) based interdigitated Metal–Semiconductor–Metal (MSM) Schottky barrier UV photodetectors. The ZnO and SZO thin films were grown on p-type silicon (Si) (100) substrates by sol-gel and spin coating technique. The three devices were fabricated using silver (Ag) as Schottky contact photodetectors based on un-doped ZnO, SZO with (2% and 4%) doping ratios. The structural and morphological properties of ZnO and SZO thin films were studied using Scanning Electron Microscopy (SEM), X-ray diffraction (XRD), and Atomic Force Microscopy (AFM). The optical and electrical properties for these films were studied using UV-visible and Hall effect measurements. With the applied voltage in the range of (-5 to 5 V) under dark condition, the values of the saturation current, barrier height, ideality factor, reach through and flat band voltages were extracted. Under UV illumination with different optical power levels ranging from (163.2µw -171.8µw) with a wavelength (254 nm), the values of the photo current, contrast ratio, responsivity, quantum efficiency, detectivity, and noise equivalent power were extracted. The SEM images showed a non-uniform distribution of the Ag dopants, these dopants were formed clusters and this clusters increased as the amount of Ag dopants increased. The mobility, carrier concentration, and roughness for the SZO films were increased as compared with undoped film. The optical band gap and the transmittance were decreased with increasing in the doping ratio. It was found that the saturation current decreased by a factor of 4, and 12 for the devices based on Ag doped ZnO (with 2% and 4 %) doping ratio. The sensitivity was significantly increased with increasing in doping ratio. This enhancement attributed to the roughness of the Ag doped ZnO thin films. Thus, this study revealed that the Ag doped ZnO films resulted in devices exhibiting better photoresponse as compared to those using un-doped ZnO thin films.

Keywords*: ZnO, SZO , ZnO:Ag, MSM, UV , Sol-gel, Ag.*

التأثيرات الكهربائية والضوئية لتطعيم الفضة للغشاء الرقيق لأوكسيد الخارصين ككواشف ضوئية للاشعة فوق بنفسجية نوع معدن-شبه موصل-معدن

الخلاصة: يتناول هذا البحث تصنيع و توصيف وتحليل اداء ثنائي متحسس اشعة فوق البنفسجية نوع (معدن - شبه موصل - معدن) باستخدام اغشية اوكسيد الزنك الرقيقة النقية والمشوبة بالفضة بلنسب (2 و4%) على قاعدة سليكون نوع موجب باستخدام تقنية البرم المغزلي، تم تصنيع الاجهزة الثلاث باستخدام معدن الفضة كأقطاب شوتكي. تمت دراسة الخصائص التركيبية للاغشية الرقيقة والمشوبة باستخدام المجهر الالكتروني الماسح، جهاز حيود الاشعة السينية، مجهر القوة الذرية . تمت دراسة الخصائص البصرية والكهربائية باستخدام قياس تاثير هول وقياس طيف الامتصاص. تمت دراسة الخصائص الكهربائية للاجهزة المصنعة باستخدام نظام توصيف شبه الموصل (semiconductor characterization system) في درجة حرارة الغرفة. الفولتية المسلطة كانت ضمن المدى (-5 to 5 V). تمت دراسة خصائص (التيار-فولتية) للاجهزة في حالتين، تحت تاثير الظلام و تحت تاثير

* *Ghusoon.ali@gmail.com*

الاشعة فوق النفسجية لعدة مستويات من الطاقة ضمن المدى (163.2 to 171.8 µw) باستخدام مصدر للاشعة فوق البنفسجية بطول موجي 254 نانومتر. تحث تاثير الظلام تم استخلاص تيار الاشباع، ارتفاع حاجز شوتكي، معامل المثالية، الفولتيات reach through, flat band. تحت تاثير الاشعة فوق البنفسجية ولعدة مستويات من الطاقة تم استخلاص تيار الفوتون, الحساسية، الاستجابية، الكفاءة الخارجية الكمية، الاكتشافية، طاقة الضوضاء المكافئة. بينت صور المجهر الماسح الالكتروني، توزيع غير منتظم لشوائب الفضة، هذه الشوائب كونت عناقيد وهذه العناقيد زادت مع ازدياد نسبة التشويب. زادت الحركية، تركيز حاملات الشحنة، والخشونة للاغشية المشوبة مقارنة بالاغشية غير المشوبة. قلت فجوة الطاقة والنفوذية للاغشية المشوبة مع ازدياد نسبة التشويب.. تبين من خلال الدراسة ان تيار الاشباع يقل بمقدار 4 مرات عند نسبة التشويب 2% ويقل بمقدار 12 مرة عند نسبة التشويب 4%. العلاقة بين الاستجابية والفولتية كانت غير خطية وهذا يوكد بان الاجهزة المصنعة لها سلوك شوتكي. التشويب بالفضة يودي الى زيادة الحساسية للاجهزة المصنعة. الاكتشافية كانت عالية للاجهزة التي غشائها الرقيق مشوب بالفضة مقارنة مع حالة عدم التشويب. عند مقارنة الاداء للاجهزة المصنعة تبين ان التشويب بالفضة يعطي اداء افضل مقارنة مع حالة عدم التشويب.

1. Introduction

ZnO is a II-VI material with sole semiconducting, piezoelectric and photoconducting, properties. This mixture of properties makes zinc oxide attractive for use in optoelectronic and sensor devices. ZnO has wide band gap (3.3 eV at 300 K), high exciton binding energy of 60 meV, high melting and boiling points. It is non-toxic material, cheap, chemically stable, and has high resistance to high radiation energy [1-3]. As grown, ZnO is generally n-type, because of the absence of stoichiometry by the presence of native donor defects, hydrogen defects, oxygen vacancies and or zinc interstitials [4]. Stable p-type doping with different materials such as Lithium (Li) and Nitrogen (N) has been attempted but remains a major hurdle to the full utilization of p-type zinc oxide [5-7]. ZnO films can be prepared by different methods, such as sputtering, and pulsed laser deposition, molecular beam epitaxy, and recently by sol–gel technique [8-11].

In other hand, Schottky Metal Semiconductor Metal (MSM) photodetector (PD) has many advantages, such as low capacitance, high speed of operation, compatible with planer FET, simplicity of fabrication, planer technology, and high sensitivity [3]. To achieve high performance photodetector, a large Schottky barrier is necessary. The large barrier leads to small dark current and an improvement in the photocurrent to dark current contrast ratio [12]. The responsivity and quantum efficiency can be increase by increasing the light trapping capability of the active layer by utilizing optical enhancement effects. This can be achieved by trap photo-induced charge carriers (by doping the active layer). There have been numerous investigations on the effect of doping on the performance of the metal–semiconductor–metal (MSM) structure based on ZnO films [13,14]. A. Ievtushenko et al. [13] demonstrate a significant improvement in the rectification ratio (~ 100 at bais 1 V) for Nitrogen doped ZnO (N:ZnO) with maximal responsivity of 0.1 A/W. They attributed this enhancement to the positive nitrogen role in suppression of crystal lattice defects in ZnO formed by oxygen vacancies. Zhonget al. [14] have demonstrated that with 3% Pd-doped ZnO the photoresponse could significantly improve, which they attribute to the high separation rate of the carriers and the increasing in the adsorption ability of light. However, there are no reports on the study of Ag dopant effects on electrical and optical properties of Ag: ZnO films based Metal Semiconductor Metal (MSM) PDs.

In the present study, we present the fabrication and characterization of Ag Schottky contact based on un-doped ZnO and Ag doped ZnO MSM photodetetectors. The electrical characteristics

and optical response of the devices were studied and compared to explore the potential application of these configurations as UV photodetectors.

2. Experimental Work

Fig. 1 shows a schematic diagram of the MSM photodetector geometry for the devices structures under study: devices based on (a) un-doped ZnO, (b) Ag-doped ZnO. The deposition of the ZnO and SZO thin films active layers was carried out by using the sol–gel technique.

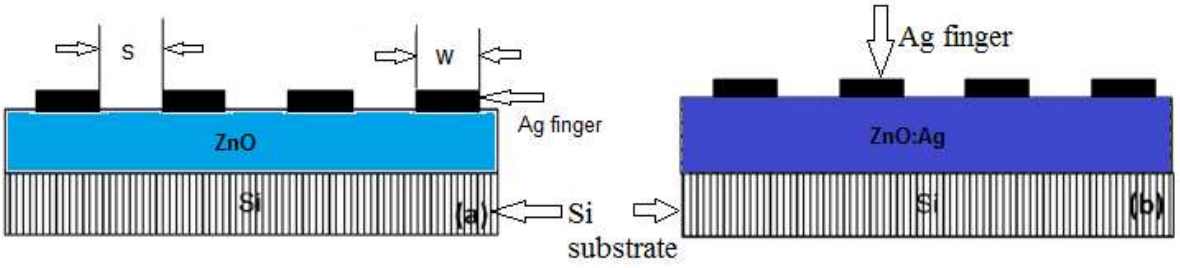

Figure 1. Schematic diagram of the MSM photodetector geometries for devices based on (a) un-doped ZnO films, (b) ZnO:Ag films

2.1. *Sample Preparation*

The substrates used in this works were cleaned using the liquid cleaning method [11]. The substrates used for deposition were p-type Si (100) (380 μm thick) with a resistivity of 2–7 Ω cm and glass substrates for UV-vis absorption technique (transparent substrate). Several steps used to cleaning the Si substrates, The first step was immersed the substrates in trichloroethylene on ultrasonic bath for 5 min, then in acetone for 1 min. the second step was done by putting the substrates in a solution consisting of 60% H_2O_2 and 40% H_2SO_4 to remove the organic residues, after that again in acetone for 2 min, and deionized water DI (resistivity 18MΩ.cm) for 3 min, and then in dry air to remove the liquid from the substrates, the last step the substrates was quenching in a beakers. After that, the substrates were ready for growth.

Zinc acetate dehydrate was the starting material for the preparation of ZnO and SZO sols for coatings in this technique. Zinc acetate dehydrate has many advantages as associated with alkoxides like zinc-n-propoxide such as, low cost material and good solubility in alcohols. However, in the absence of other agents or heating, zinc acetate dihydrate has only limited solubility in alcohols. For un doped solution, 0.4 mol/l concentration of zinc acetate dehydrates $(Zn(CH_3COO)_2.2H_2O{:}ZnAc_2.2H_2O)$ was prepared by dissolving 1.75 g of zinc acetate in a solution containing 0.8 g diethanolamine (DEA: $[CH_2(OH)\,CH_2]_2NH$) and 20 ml isopropanol ($(CH_3)_2CHOH$) at room temperature (300 K). The DEA to zinc acetate molar ratio was kept to 1:1 [11]. Two solutions for Ag-doped ZnO were prepared. The first solution consists of 0.02 mol/l concentration of silver acetate $AgC_2H_3O_2$ prepared by dissolving 0.13 g of silver acetate in a solution of isopropanol and desired amount of DEA. The second solution consists of 0.04 mol/l

of silver acetate concentration prepared by dissolving 0.06 g of silver acetate in a solution of isopropanol and desired amount of DEA [11]. Both the first and second solutions of Ag doped were mixed with 1.75 g of zinc acetate dihydrate dissolved in 0.8 g DEA and 10 ml isopropanol. Finally the solutions were stirred using magnetic stirrer (model Y-HS11) for 1 h at room temperature to produce a clear, transparent, and uniform solution which could be used for coating. The prepared solutions were deposited on the substrates using spin coater (model Chemat technology KW). The substrates were silicon and glass (for UV absorption). The substrates were spin coated for 60 s at a speed of 4000 rpm, then drying the thin film at 100° C by using Muffle furnaces for 10 min. The drying process was used to remove organic residuals and to evaporate the solvent from the films and then the samples were annealed at 450 °C using a furnace (model KSL-1100 X MTI) for 1 h to produce the thin films.

The software that was used to design the interdigitated mask was AutoCAD software. The mask consists of 10 fingers with a length (L) of L=1800 μm and width (W) of W=200 μm, and an inter-electrode spacing (S) of 200 μm. The fabrication of the mask was done by Wire Electrical Discharge Machining (WEDM). Ag electrodes (thickness 100nm) with high purity (99.99%) were deposited on the prepared thin films to form Schottky contact and this was done by fixing the fabricated mask on the thin film and putting it inside the deposition unit using Vacuum thermal evaporator system (model thermionics V 90).

2.2. *Characterization*

The crystal structures of the ZnO and SZO films were characterized by X-ray diffraction (XRD) using X-ray diffractometer (Shimadzu XRD- 6000), to estimate lattice constants, grain size, dislocation density, and the orientation. The surface topography of the samples such as the surface roughness, the grain size was measured by using atomic force microscope AFM (AA3000 Scanning probe microscope) and by Scanning Electron Microscope (SEM) (Vega3 Tescan).

For the investigation of the carrier concentration, resistivity, and mobility, Hall effect measurement was done using an Ecopia (HMS 300). The absorbance spectra of ZnO and SZO films were studied by using (UV-1650 UV-Visible Recording Spectrophotometer) in the wavelength range from 200 to 1100 nm. The thicknesses of the un-doped ZnO, ZnO:Ag films were estimated to be in the range of 146 nm as measured by TF Probe.

The fabricated MSM PDs was characterized using Keithley Semiconductor Characterization System (SCS) (model 4200-SCS), made in USA at room temperature (27 °C). The applied voltage was between -5 V to 5 V under dark and illumination conditions. A UV lamp with a wavelength 254 nm (model UVC-D215T5 6W) was used for illumination with optical power meter. The UV illumination power levels were ranging from 163.2 μw to 171.8 μw. The Shottky parameters such as the leakage current, barrier height, reach through voltage, flat band voltage and ideality factor were estimated from dark current condition. While the performance parameters such as the photocurrent, contrast ratio, responsivity, detectivity, noise equivalent power were extracted under illumination condition.

3. Results and Discussion

Figs. 2(a–c) show SEM micrographs of the films structures, Fig.2 a shows smooth and uniform undoped ZnO film, Figs.2 (b and c) show the Ag dopants were agglomerated and form a clusters (particles), which are in inhomogeneous distribution through ZnO film. The images also show that, these particles become denser with increasing the doping concentration, no visible surface crack.

It is quite evident that there is no definite morphology in the samples. It is also clear from Fig.2 (b and c) that the SZO films have greater surface roughness than undoped ZnO. These clusters also increased the sensitivity of SZO based UV MSM PDs since the incident light scattered inside the active area for the fabricated devices and as result the photocurrent for SZO based thin film was increased. Fig.2 (d-f) shows the AFM images for the fabricated devices. The grain size of ZnO and SZO thin films was found to be decreased with the increasing in the doping concentration.

The decreased grain size results in an increase in mobility value [12]. The increasing of mobility may be attributed to Ag dopant. These Ag clusters in the SZO (shown in SEM) are acts as electron path and as a result the mobility of SZO is increased [11]. The roughnesses of doped ZnO films are larger than un-doped one.

The grains sizes were 59.28, 44.37, and 40.68 nm for ZnO, ZnO:Ag 2% and ZnO:Ag 4% thin films respectively. As the roughness of the films increased in SZO thin films, the surface to volume ratio was increased, and this will increase the probability of the electron hole pair generation when the light is applied on the device [13]. The large area to volume ratio (roughness) for the doped films also decreased the carrier transient time and increased the carrier life time. As result total transfer charge was increased and the photocurrent is amplified [14].

Fig.3 shows XRD spectrum for the un-doped ZnO, Ag:ZnO 2%, and Ag:ZnO 4%, thin films respectively. It can be seen that the diffraction peaks for undoped and Ag doped films show a polycrystalline hexagonal wurtzite crystal structure. Fig.3 (a, and b) shows five peaks of the hexagonal ZnO crystal structure, these peaks appear at 2θ from 30◦ to 60◦ that correspond to the (100), (002), (101), (012), and (110) orientations. There was no dominant peak, and the peak of the silicon substrate was observed at 69◦ (400) orientation.

Two peaks (012 and 110) were vanished with increasing in doping ratio at 4% as shown in Fig.3 c. The full width at half maximum (FWHM) of thin films was from 0.302°-0.677°, the small values of FWHM causes the good crystallinty.

It is clear from Fig.3 when the Ag doping ratio increased a slightly shift with 2θ towards small values i.e., an increment with d_{hkl} (due to placed Ag ions into ZnO lattice). As a result the lattice constants of the Ag doped thin films were increased because the Ag dopants. Since the Ag ions have big radius (122 pm) which is greater that the Zn+ ion radius (72 pm), so it can be concluded that the big Ag ions were substituted into the Zn+ in the silver doped zinc oxide crystal.

According to this substitution, the intensity of the peaks slowly reduced as the amount of Ag dopant increased. The diffraction peaks corresponding to the reflections of crystal planes obtained for all the films are in consistent with JCPDS data of ZnO (Card no. 96-901-1663).

The electronic parameters were measured by van der Pauw and Hall methods, the results shows that the deposited ZnO thin film is n-type semiconductor, silver doping also significantly increased the electron concentration, making the films heavily n-type. The mobility for the SZO increased as mentioned before because Ag dopant which acts electron path. The resistivity decreased with increasing in the doping ratio which can be attributed to the increase in the carrier concentration and mobility. The fabricated SZO thin films do not show p-type, the reason may be the working temperature (annealing) is high [15].

Instead of p-type behavior, the fabricated SZO thin films show the properties of n-type semiconductor and the conductivity was in continuously increased.

The bandgaps of ZnO and SZO were evaluated from the absorbance spectra of ZnO and SZO obtained by using double beam spectrophotometry in the wavelength range from 100 to 1100 nm. The optical bandgaps of ZnO and SZO thin films were estimated by using the following fundamental relation,

$$\alpha hv = B(hv - Eg)^{n}, \qquad (1)$$

where α is the absorption coefficient, hv is the energy of absorbed light, n =1/2 for direct allowed transition, and B is the proportionality constant. The energy bandgap (Eg) was obtained by plotting $(\alpha hv)^2$ versus hv and extrapolating the linear portion of $(\alpha hv)^2$ versus hv so as to cut the hv axis as shown in Fig. 4. The band gaps were 3.25, 3.20 and 3.12 eV for ZnO and SZO thin films respectively. The small decrease in band gap with the increasing in the doping ratio may be due to the splitting of the energy levels near the Fermi level and this splitting because of the atomic hybridization between the Ag atom and its neighboring O atoms.

The band gap of SZO films should be smaller than the band gap of ZnO films because the band gap of AgO (bulk value 1.2 eV) is lower than that of ZnO (bulk 3.4 eV), which result in splitting the energy levels. Table 1.1 summarizes the major parameters obtained from thin films characterization.

Table 1.1 The parameters obtained from thin film characterization.

Parameters	ZnO	ZnO:Ag 2%	ZnO:Ag 4%
Roughness (nm)	0.0224	0.0673	0.0369
grain size (nm)	59.28	44.37	40.68
Film thickness (nm)	146	146	149
Resistivity (Ω.cm)	131	17	0.27
Mobility ($cm^2\ V^{-1}s^{-1}$)	18	88	46
Bandgap (eV)	3.25	3.21	3.12
Carrier concentration(cm^{-3})	2.5×10^{15}	4×10^{15}	5×10^{17}

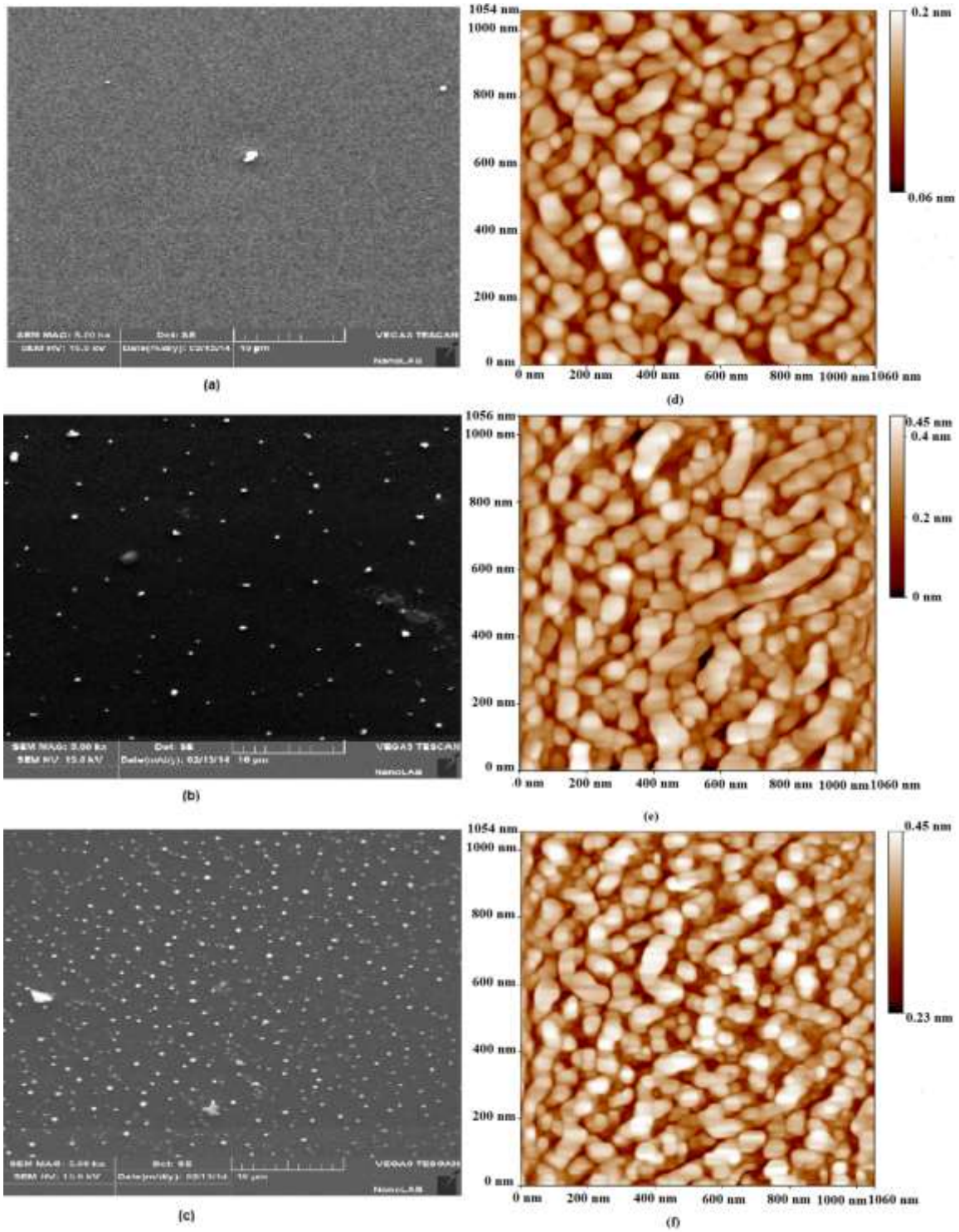

Figure 2. (a) SEM image of un-doped ZnO film. (b) SEM image of ZnO:Ag 2 % film. (c) SEM image of ZnO:Ag 4 % film.(d) 2D AFM image of un-doped ZnO film. (e) 2D AFM image of ZnO:Ag 2% film.(f) 2D AFM image of ZnO:Ag 4% film.

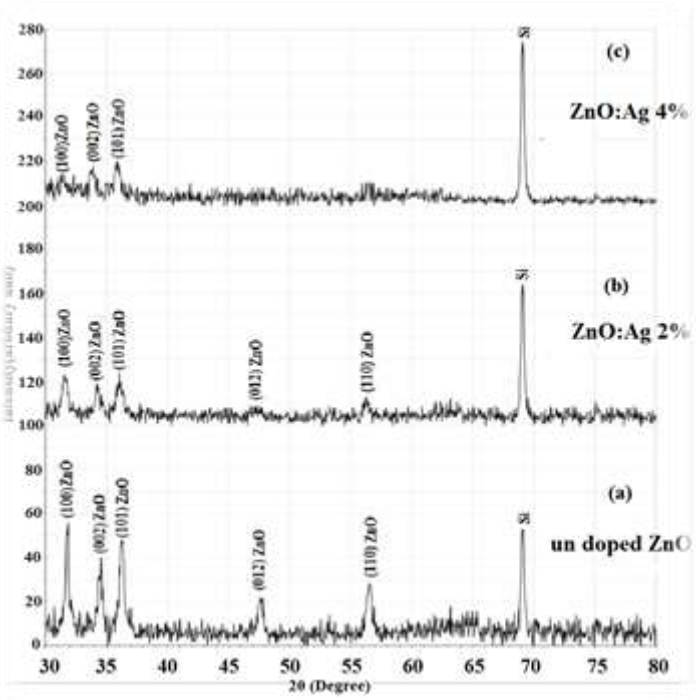

Figure 3. XRD spectrum for ZnO thin films with different doping ratio deposited on Si (100) substrate, (a) un doped ZnO , (b) 2% Ag, (c) 4% Ag.

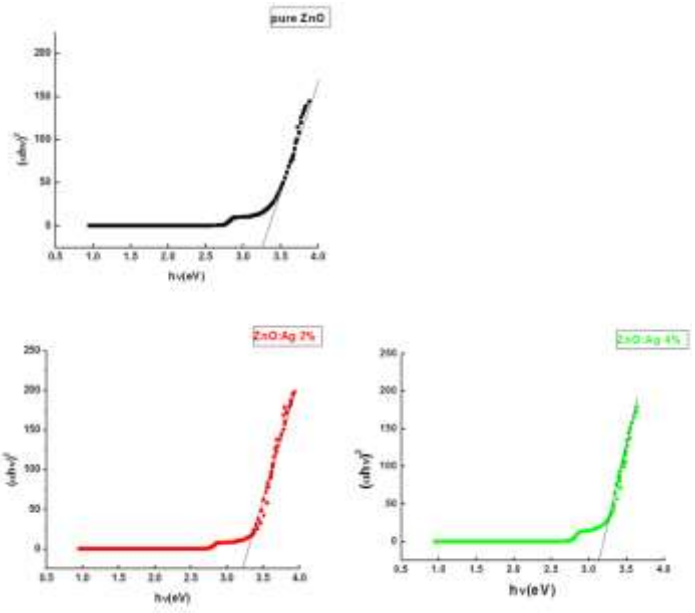

Figure 4. $(\alpha h\upsilon)^2$ versus $h\upsilon$ for estimation the bandgap of the ZnO film deposited on Si substrate p-type <100> by sol gel and spin coating technique (a) ZnO, (b) ZnO:Ag 2%, (c) ZnO:Ag 4%.

Fig.5 shows the I-V characteristics under dark condition at room temperature (300 K), it was clear that the three MSM PDs based on ZnO and SZO with (2 and 4%) doping ratios films were worked as a Schottky diode. The dark current characteristics consist of three regions of operation

depending on the applied voltage on the MSM PD, these regions were; (1) before V_{RT}, (2) between V_{RT} and flat band voltage V_{FB} (3) past V_{FB}. From Fig.5 (b and c) after V_{FB}, a small increase in the current with the applied bias was observed, and no indication of saturation current and this be in good agreement with previous reports [16-17]. The presence of an interfacial layer between the silicon substrate and SZO semiconductor due to silver doping may be the cause for this increasing. The dark currents at 3 V were 2.44×10^{-6}, 1.23×10^{-6}, and 5.5×10^{-7} A for the devices based on ZnO and SZO with (2 and 4%) doping ratio films, respectively. It can be seen at 3V that the dark current decreased by a factor of 2 for ZnO: Ag 2% PD, and decreased by a factor of 4 for ZnO: Ag 4% PD, as compared with un doped ZnO PD. It is well known that there is a relation between the concentration of the carriers in the semiconductor (known from Hall effect measurement) and the voltages (V_{FB} and V_{RT}). It can be noticed that when the concentration of carriers increased, the depletion layer width decreased, and as a result the V_{RT} and V_{FB} voltages decreased.

The relation between the carrier concentration and the voltages is shown in table 2. The metal semiconductor metal PD is essentially consists of two Scottky contacts connected back to back on semiconductor substrate. Thermionic emission theory can be used to describe the current across the Shottky diode [11], for low voltage the current can be given by,

$$I = \left[AA^{*}T^{2}\exp\left(\frac{-q\Phi_b}{kT}\right)\right]\left[\exp\left(\frac{qV}{nkT}\right)-1\right], \qquad (2)$$

where n is the ideally factor, q is the element charge, k is the Boltzmann's constant, T is the absolute temperature, Φ_b is the barrier height, A is the area of the Schottky and A* is the effective Richardson coefficient ~32 A/cm²K².

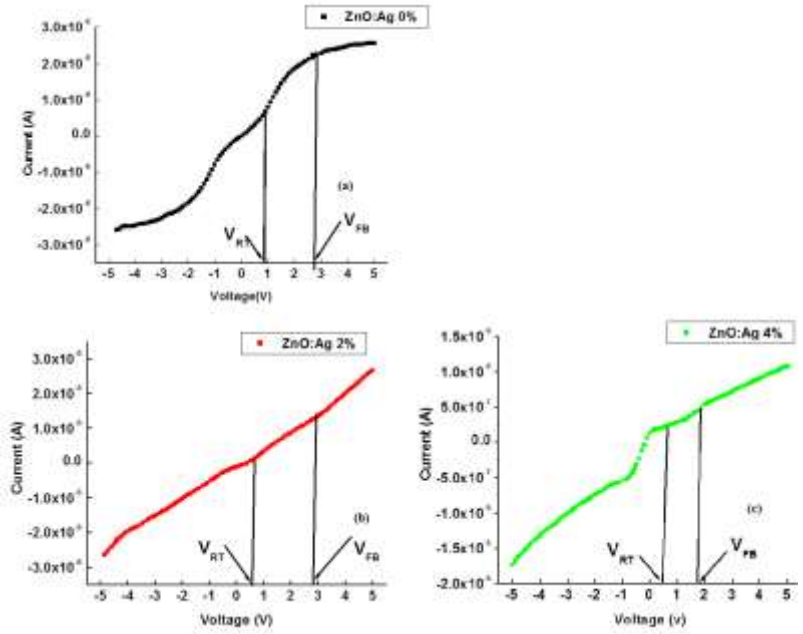

Figure 5. I–V response for (a) Ag/ZnO,(b) Ag/ZnO:Ag 2%, (c) Ag/ZnO:Ag 4%, ZnO photodetectors.

Table 2 The correlation between the carrier concentration and the voltages for ZnO and SZO based MSM PDs.

Parameters	ZnO	SZO 2%	SZO 4%
Carrier concentration (cm^{-3})	2.5×10^{15}	4×10^{15}	5×10^{17}
Reach through voltage (V)	0.95	0.7	0.5
Flat band voltage(V)	2.9	2.9	1.9

For all the voltages applied to the fabricated MSM PDs, the term $\exp\left(\frac{qV}{kT}\right)$ was much greater than 1, so equation 2 can be approximated as,

$$I = I_s \exp\left(\frac{qV}{nkT}\right), \quad (3)$$

where

$$I_S = AA^*T^2 \exp\left(\frac{-q\Phi_b}{kT}\right), \quad (4)$$

The saturation current can be found by extrapolation of the dark current (equation 4.11) at zero voltage [18].The saturation currents were 7.4×10^{-7}, 2×10^{-7}, and 6×10^{-8} A, for the devices based on un-doped and doped (with silver 2% and 4%) respectively.

The saturation current decreased by a factor of 4 for the device based on 2% Ag doping and decreased by a factor of 12 for the device based on 4% Ag doping and this enhanced the barrier height. The barrier height can be found by taking the natural logarithm to equation 4 that yields,

$$\Phi_b = \frac{kT}{q} \ln\left(\frac{AA^*T^2}{I_s}\right), \quad (5)$$

The barrier heights were found to be around 0.68, 0.709, and 0.74 eV for ZnO, SZO 2%, SZO 4% MSM PDs respectively. The barriers heights that were founded are larger than the theoretical values and this may be due to silver oxide which plays a role in the contact structure since Ag Schottky contact tended to "improve with age" [18].

Another reason was the increasing of surface states trapping in the SZO films, the barrier height doesn't depend on the metal work function if the density of the surface states is large. To estimate the ideality factor, the natural logarithm of equation 3, is

$$n = \frac{qV}{KT} \ln\left(\frac{I}{I_s}\right), \quad (6)$$

so the ideality factor is a function of voltage. At low voltages, the values of the ideality factor were found to be 1.4, 1.8 and 2 for the devices based on ZnO and SZO, respectively. These large values for the ideality factor mean that the current in the devices cannot be described by thermionic emission theory alone. Other mechanisms should be taken in to account such as the tunneling transport through the barrier and the existence of surface states at the surfaces of the

thin films [19]. The films were used in this study were interfacial layers with thicknesses 142 ~146 nm including the adsorbed oxygen, hydroxide, etc, on the surface of these films. One can noticed that as the doping ratio was increased, the absorbed oxygen and hydroxide was also increased. Due to this increasing a large density of surface states occurred at the semiconductor. Subsequently, a band bending with a potential barrier was formed at the surface of ZnO and SZO films. Because of the pinning of the Fermi energy from the surface states, the barrier that was formed was nearly independent of the work function of the metal. The surface states can be controlled the barrier height if its density is high enough. However there is no mechanism to control the presence of these surface sates. So lager value of the surface states lead to non-ideal diode characteristics with a large value of ideality factor [19]. The parameters were extracted from dark-current measurement are listed in table 3.

Table.3 Barrier height, saturation current, and ideality factor for ZnO doped with Ag (Ag=0%,2%,4%) metal semiconductor metal devices.

Parameters	ZnO 0%	ZnO:Ag 2%	ZnO:Ag 4%
Barrier height (eV)	0.68	0.709	0.74
Saturation current (A)	7.4×10^{-7}	2×10^{-7}	6×10^{-8}
Ideality factor	1.4	1.8	2

For the three photodetector studied, Fig. 6 shows the photocurrent and contrast ratio (sensitivity) as a function of applied bias V measured in the air under dark and UV illumination at room temperature (300 K).

The photocurrent is defined as the difference between the current under illumination and the dark current. Fig.6 (a-c) below shows the effect of optical power on the photocurrent for devices based on undoped, Ag doped (with 2% and 4% doping ratio). The maximum photocurrent was 1.2×10^{-4} A at (171.8 µw) for applied voltage 5V for Ag/ZnO:Ag 4% sensor.

The high photocurrent in ZnO:Ag 4 % thin film based MSM PD was due to a large presence of oxygen related trap states at the thin film surface, the high surface trap states prevents the recombination of charge carrier and extends the life time of holes.

The large area to volume ratio in ZnO: Ag 4% with smallest grain size (40 nm) and the existence of deep level surface trap made the photocarrier life time longer. Fig.7 shows the photocurrent versus the optical power at 5 V, it can be noticed that the highest photocurrent was in ZnO:Ag 4% PD.

The contrast ratio S_{UV} was calculated by the following equation,

$$S_{UV} = \frac{I_{ill}}{I_{dark}}, \qquad (7)$$

where I_{dark} is the current under dark condition, and I_{ill} is the current under illumination at a certain level of optical power. It can be seen that as the optical power increased, the sensitivity increased in the negative and positive directions of applied bias.

When the bias voltage reached the flat band voltage V_{FB}, the sensitivity decreased until saturation. The maximum sensitivity occurred when the photodetectors operated at flat band bias conditions for the three devices.

For device based on ZnO active layer, the sensitivity remains relatively constant after 3 V, while the other devices based on Ag doped ZnO active layers the sensitivity reaches its maximum at V_{FB} and then decreased. The maximum contrast ratio at 171.8μW were 6.7, 37, and 39 for ZnO and SZO 2%, SZO 4% based MSM PDs respectively. Devices based on ZnO:Ag films show an order of magnitude improvement in sensitivity.

This improvement in the sensitivity because of the increasing of oxygen related hole trap states at the SZO thin films surfaces. Fig.8 shows the maximum sensitivity at V_{FB} for the three devices as a function of optical power. From Fig.8 , one can noticed that the sensing capability to UV illuminations is in significantly increasing with increasing in the optical power levels for the devices based on Ag doped ZnO films as compared with the device based on ZnO film.

The suggestion is that the sensing mechanism was improved due to the incorporation of Ag dopants in the active layer of ZnO semiconductor.

The optical to electrical (O/E) conversion efficiency is measured by the external quantum efficiency given by equation,

$$\eta_{ext} = \frac{I_{Ph}}{P_{opt}} \times \frac{h\nu}{q}, \qquad (8)$$

where h the Planck's constant and ν is the frequency of the light. Although Schottky MSM PDs are not expected to have a gain due to the presence of Schottky contact which prevents the secondary charge carriers. Sometimes there is a gain G, so when EQE exceed 100%, the EQE become 1 and a gain G detected in the photodetector.

In this study it was found that Ag/ZnO:Ag 2%, and Ag/ZnO:Ag 4% detectors have gain equal to 108%, and 250% respectively. The quantum efficiencies (or gain in SZO (2 and 4 %) based ZnO) increased with increasing in optical power levels.

The maximum efficiencies of the studied devices were 44%, 108% and 250%, for devices based on un-doped, doped with 2% Ag, and doped with 4% Ag, respectively. The external quantum efficiency for Ag/ZnO PD and the gain for Ag/ SZO are shown in Fig.9.

It is clearly seen from Fig.9 that the EQE starts to increase with increasing in optical power levels, no saturation in EQE, suggested that more optical power need to get the saturation.

The gain in the Ag doped devices depends on the surface states of the thin films, as the surface traps increased, the gain increased.

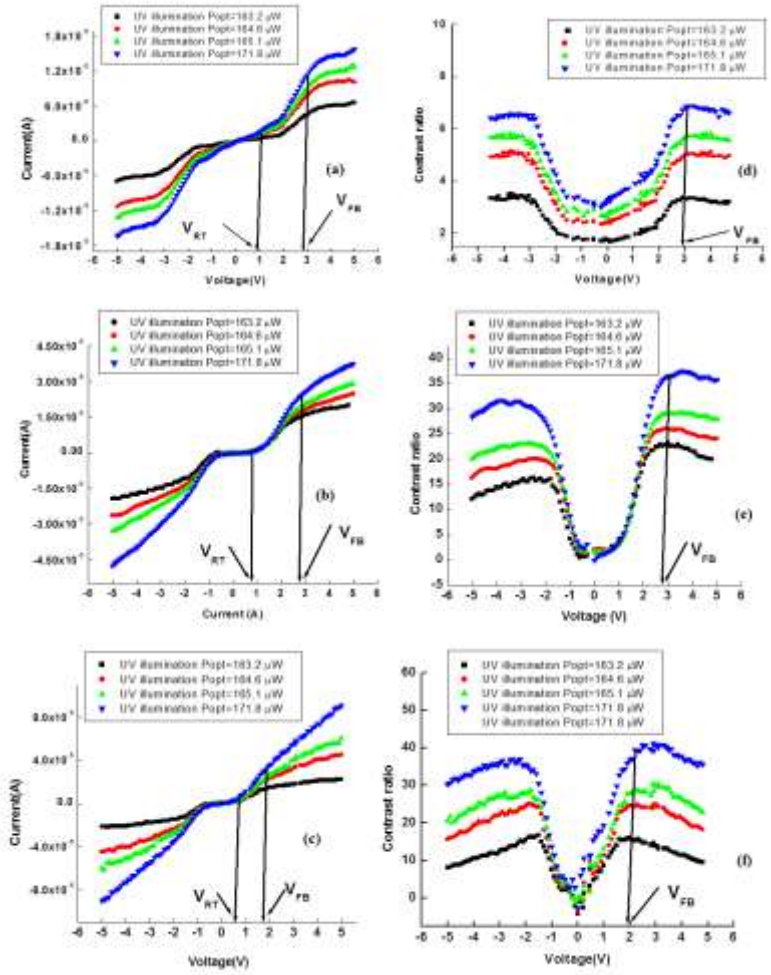

Figure 6. (a) Photocurrent vs. voltage of undoped ZnO MSM PD, (b) Photocurrent vs. voltage of ZnO:Ag 2% MSM PD, (c) Photocurrent vs. voltage of ZnO:Ag 4% MSM PD, (d) Contrast ratio vs. voltage of undoped ZnO MSM PD, (e) Contrast ratio vs. voltage of ZnO:Ag 2% MSM PD, (f) Contrast ratio vs. voltage of ZnO:Ag 4% MSM PD.

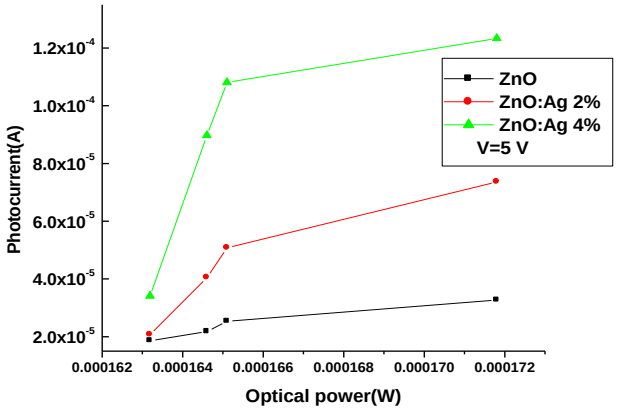

Figure 7. Photocurrent versus optical power for ZnO and SZO based MSM photodetectors with different doping ratio.

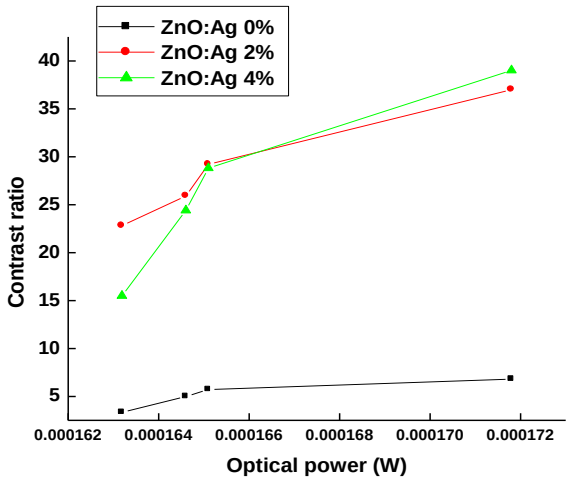

Figure 8. Maximum sensitivity at V_{FB} as a function of optical power.

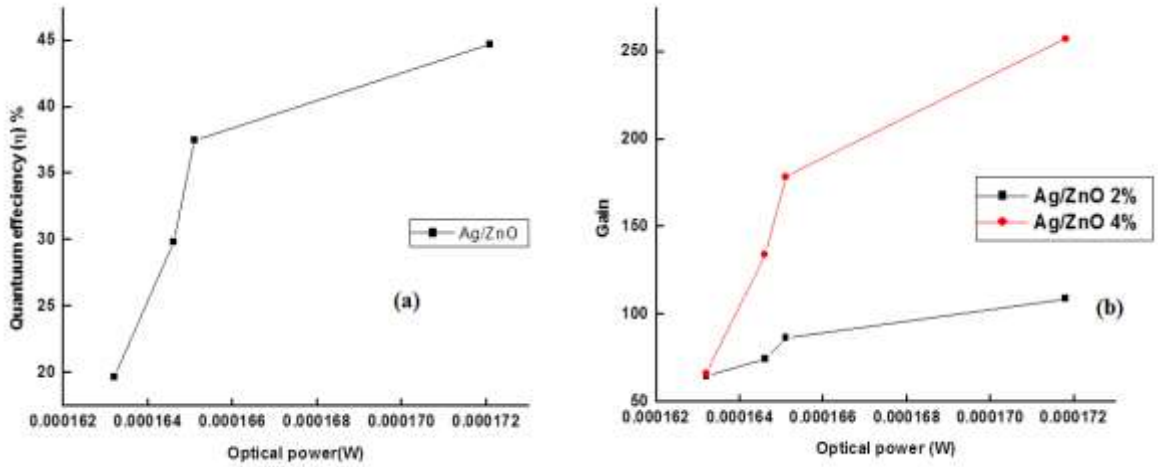

Figure 9. (a) External quantum efficiency of metal semiconductor metal for Ag/ZnO PD, (b) Gain versus optical power for Ag/ZnO:Ag 2%, and Ag/ZnO:Ag 4%/, MSM PDs.

The responsivity of the PD is relating the output current (photocurrent) to the incident optical power with different levels given in equation,

$$R = \frac{I_{ph}}{P_{opt}}, \tag{9}$$

The responsivity criteria R_{crt} of the MSM detector is given [20],

$$R_{crt} = \frac{q}{h\nu}\frac{S}{S+W}, \tag{10}$$

It can be seen that R_{crt} depends on the dimensions of the mask, finger spacing and finger width, so for 200 μm spacing and width, R_{crt} is 0.102 A/W. In the case of the PD having a gain the responsivity is given by [21],

$$R = G\frac{q\lambda}{hc}, \qquad (11)$$

The maximum responsivity for the fabricated devices (at P_{opt} =171.8 μw and V= 5V) were 0.09161, 0.2207, and 0.5269 A/W for ZnO, ZnO:Ag 2%,and ZnO:Ag 4% MSM sensors. The devices based on Ag doping (2 and 4%) were exceed the responsivity criteria R_{crt} , this means, there is a gain in the devices based on Ag doped ZnO. This gain due to the presence of oxygen related hole trap states at the thin films surface and the presence of secondary charge carrier as mentioned before. The responsivity for the fabricated devices is shown in Fig.10.

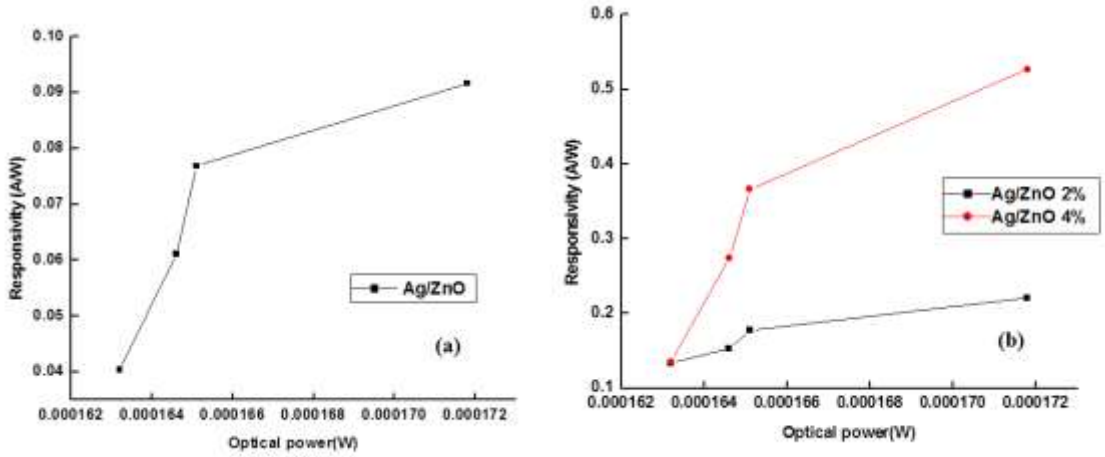

Figure 10. (a) responsivity versus optical power for Ag/ZnO and Ag/ZnO:Ag 2% MSM PDs (b) responsivity versus optical power for Ag/ZnO:Ag 4%/Ag MSM PD.

As the optical power of UV light increases, the responsivity increases also, since the photocurrent doesn't saturate due to the increasing in optical power levels, the resopnsivity will not decrease and still increasing. The highest maximum repsonsivity was observed for devices based on ZnO:Ag 4%. A nonlinear relationship between voltage and responsivity can be seen in Fig.11 and this confirms that the fabricated sensors were in Schottky contact.
The voltage dependent detectivity (D) is given by

$$D = \frac{\lambda\eta_{ext}q}{hc}\left(\frac{RA}{4KT}\right)^{1/2}, \qquad (12)$$

Where RA is known as resistance-area product of the device obtained from current density J-V characteristics. The resistance area product given in the following equation,

$$RA = (\frac{dJ}{dV})^{-1}, \quad (13)$$

By converting the measured I-V characteristics in to J-V characteristics, the zero-biased resistance-area product can be given by,

$$R_oA = \left(\frac{\partial J}{\partial V}\right)\Big]_{V=0}^{-1}, \quad (14)$$

The zero resistance area was 0.1923, 0.252, and 0.3 Ωm^2 for the devices based on ZnO and SZO with (2 and 4%) films. The maximum value for the resistance area product was in Ag/ZnO:Ag 4% PD which made this sensor suitable to use in integrated circuits. The detectivity is shown in Fig.12.

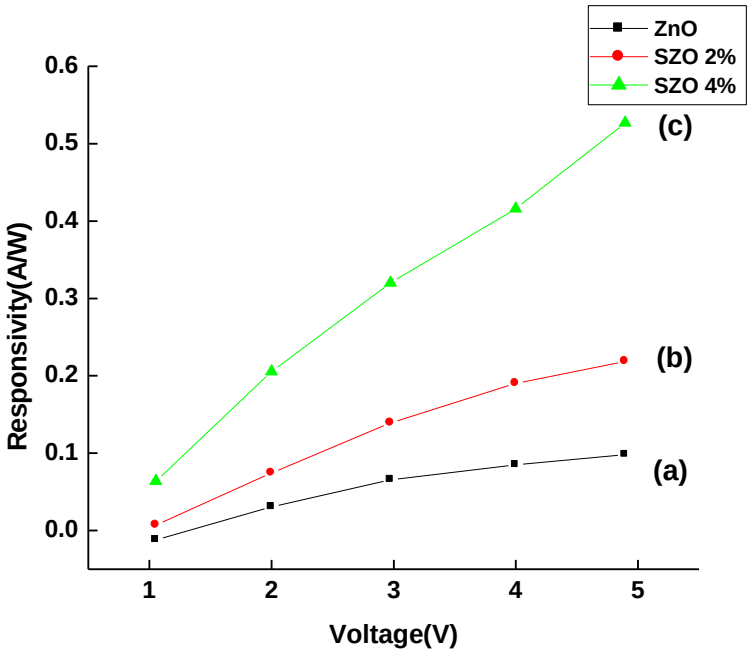

Figure 11. Responsivity verses voltage for the fabricated photodetectors, (a) Ag/ZnO, (b) Ag/ZnO 2%, and (c) Ag/ZnO 4%.

It can be seen from the figure that the detectivity was increased with increasing in the doping ratio. The maximum detectivity for the PDs was 3×10^8 , 8.6×10^8, and 2.25×10^9 $mHz^{1/2}w^{-1}$for ZnO, SZO 2% and SZO 4% PDs, respectively. The maximum detectivity was at SZO 4% based PD. The high detectivity with fairly dark current for Ag/ZnO:Ag 4% made this sensor suitable for optoelectronic applications. The noise equivalent power which is the reciprocal of the detectivity is shown in Fig.13. NEPs were extracted to be 3.3×10^{-9}, 1.16×10^{-9}, and 4.44×10^{-10} W

for ZnO, SZO 2%, and SZO 4%. From NEP, SZO 4% PD can detect a weaker signals than the others PDs.

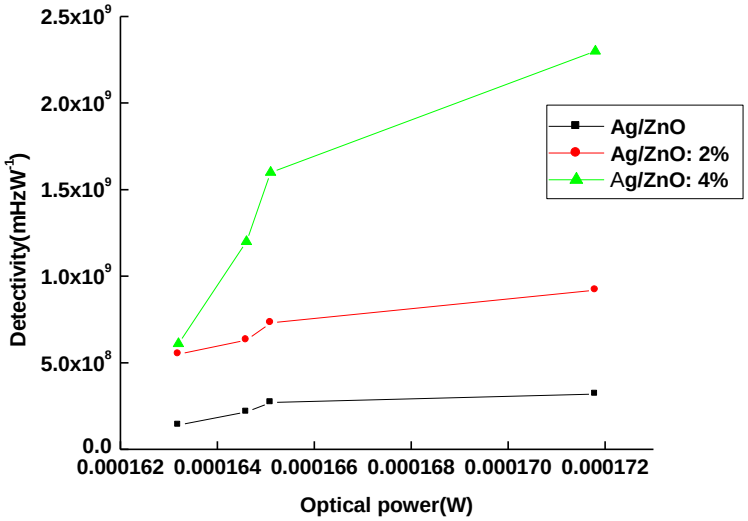

Figure 12 Detectivity for metal semiconductor metal verses Optical power, (a) Ag/ZnO, (b) Ag/ZnO 2%, and (c) Ag/ZnO 4%.

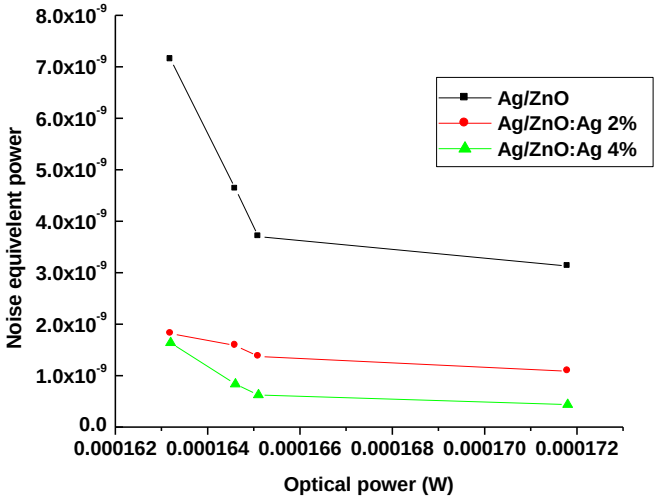

Figure.13 Noise equivalent power verses optical power for metal semiconductor metal, (a) Ag/ZnO, (b) Ag/ZnO 2%, and (c) Ag/ZnO 4%.

4. Conclusions

This paper presents the fabrication and characterization of ZnO and SZO thin films based interdigitated metal–semiconductor–metal (MSM) Schottky barrier UV photodetectors. The thin films were fabricated by using sol-gel method. The undoped ZnO film has smooth, crack free and uniform structure, while the Ag dopants in SZO film were agglomerated and form clusters

with inhomogeneous distribution through ZnO film. The saturation current was decreased for the devices based on the doped films due to increasing in the barrier heights. The sensitivity increased with doping ratio. The noise equivalent power was extracted to be 3.3×10^{-9}, 1.16×10^{-9}, and 4.44×10^{-10} W for ZnO, SZO 2%, and SZO 4%, respectively. which indicate that the SZO 4% PD can detect a weaker signals than the others PDs. The improvement in the performance of the doped films attributed to the Ag clusters since the incident light scattered inside the active area.

5. References

1. Walle, J.C. (2009). "*Fundamentals of zinc oxide as a semiconductor*". Reports On Progress In Physics. Vol.72, No.12, pp. 1-29.
2. Pearton, S.J., Norton, D.P., Heo, Y.W., and Steiner, T. (2005). "*Recent progress in processing and properties of ZnO*" Journal of Progress in Materials Science. Vol.50, pp. 293-340.
3. Grundmann, M. (2010). "*The Physics of Semiconductors; An Introduction Including Devices and Nanophysics*" Second Edition.
4. Özgüret, Ü., Alivov, Y.I, Lin, C., Teke, A., Reshchikov, M.A., Dogan, S., Avrutin, V., Cho, S.J., and Morkoc, H. (2005). "*A comprehensive review of ZnO materials and devices*" Journal of Applied Physics. Vol.98.
5. Look, D. C., and Claflin, B. (2004). "*P-type doping and devices based on ZnO*" physica status solidi (b). Vol.241, pp. 624-630.
6. Zhang, P.S., and Wei, S. (2002). "*Origin of p-type doping difficulty in ZnO: The impurity perspective*" Journal of Physical Review B. Vol.66.
7. Barnes, T.M., Olson, O.K., and Wolden, C.A. (2005). "*On the formation and stability of p-type conductivity in nitrogen-doped zinc oxide*," Journal of Applied Physics. Vol.86.
8. Lee, J.B., Kim, H.J., Kim, S.G., Hwang, C.S., Hong, S.H., Shin, Y.H., and Lee, N.H. (2003). "*Deposition of ZnO thin films by magnetron sputtering for a film bulk acoustic resonator*" Journal of thin solid films, pp. 179–185.
9. Jang, Y.R., Yoo, K.H., and Park, S.M. (2010). "*Properties of ZnO thin films grown on Si (100) substrates by pulsed laser deposition*" Journal of Material Science Technology, pp. 973-976.
10. Jin, M., Feng, J., De-heng, Z., Hong-lei, M., and Shu-ying, L. (1999). "*Optical and electronic properties of transparent conducting ZnO and ZnO:Al films prepared by evaporating method*" Thin Solid Films, pp. 98-101.
11. Ali, G.M., Moore, J.C., Kadhim, A.K., and Thompson, C. (2014). "*Electrical and optical effects of Pd micro plates embedded in ZnO thin film based MSM UV photodetectors: A comparative study*" Journal of Sensors and Actuators. Vol.209, pp.16-24.
12. Lin, T.K., Chang, S.J., Su, Y.K., Huang, B.R., Fujita, M., and Horikoshi, Y. (2005). "*ZnO MSM photodetectors with Ru contact electrodes,*" Journal of Crystal Growth. Vol.281, No.2, pp. 513-517.

13. Lashkarev, I.G., Lazorenko, V., Ulyashin, A., Karpyna, V., Sichkovskyi, V., and Khranovskyy, V. (2008). "*Ultra violet detectors based on ZnO:N thin films with different contact structures*" Journal of Acta Physica Polonica A. Vol.114, pp.1123-1129.
14. Zhong, J.b., Li, J., He, X., Zeng, J., Lu, Y., Hu, W., and Lin, K. (2012). "*Improved photocatalytic performance of Pd-doped ZnO*" Journal of Current Applied Physics. Vol.12, No.3, pp. 998–1001.
15. Lugo, F. (2010). "*Synthesis and characterization of Silver doped Zinc Oxide thin films for optoelectronic devices*" PhD thesis, University Of Florida, Graduate School.
16. Chuah, L.S., Hassan, Z., and Abu-Hassan., H. (2007). "*Dark current characteristics of Ni contacts on porous AlGaN-based UV photodetector*" Journal of Optoelectronic and Advanced Materials. Vol. 9, No.9, pp. 2886–2890.
17. Averine, S., Chan, Y.C., and Lam, Y.L. (2000). "*Evaluation of Schottky contact parameters in metal-semiconductor-metal photodiode structures*" Journal of Applied Physics. Vol.77, No.2.
18. Allen, M.W., and Alkaisi, M.M. (2006). "*Metal Schottky diodes on Zn-polar and O-polar bulk ZnO*" Journal of Applied Physics Letters. Vol.89, No.10.
19. Ali, G.M., Thomson, C.V., Jasim, A.K., and Abdlbaqi, I.M. (2013). "*Effect of embedded Pd microstructures on the flat-band-voltage operation of room temperature ZnO-based liquid petroleum gas sensors*" Sensors, pp. 16801-16815.
20. Duboz, J.Y., Reverchon, J.L., and Adam, D. (2002). "*Submicron metal-semiconductor-metal ultraviolet detectors based on AlGaN grown on silicon: results and simulation*" Journal of Applied Physics. Vol. 92, No. 9, pp. 5602-5604.
21. Sze, S.M., Ng, K.K. (2007) "*Physics of Semiconductor Devices*" Third Edition.